Short communication

Reactive uptake of ammonia by secondary organic aerosols: Implications for air quality

Jeremy R. Horne[a], Shupeng Zhu[a], Julia Montoya-Aguilera[b], Mallory L. Hinks[b], Lisa M. Wingen[b], Sergey A. Nizkorodov[b], Donald Dabdub[a,*]

[a] Computational Environmental Sciences Laboratory, Department of Mechanical & Aerospace Engineering, University of California, Irvine, Irvine, CA, 92697, USA
[b] Department of Chemistry, University of California, Irvine, Irvine, CA, 92697, USA

ABSTRACT

Reactions between ammonia (NH_3) and organic compounds containing carbonyl functional groups in aerosol particles can form organic products that are less basic than NH_3 and are thus unable to neutralize efficiently nitric and sulfuric acids. In this exploratory study, the University of California, Irvine - California Institute of Technology (UCI-CIT) model is used to investigate the potential air quality impacts of including of the chemical uptake of NH_3 by secondary organic aerosols (SOA) in a regional airshed model. A surface reaction of NH_3 with SOA is implemented into the model to determine the impact of this process on NH_3 and $PM_{2.5}$ concentrations in the South Coast Air Basin of California (SoCAB). Air quality simulations are conducted using uptake coefficients ranging from 10^{-5} to 10^{-2} to explore the sensitivity of changes in NH_3 and $PM_{2.5}$ concentrations to the magnitude of the uptake coefficient. Results indicate that the chemical uptake of NH_3 by SOA can potentially deplete gaseous NH_3 concentrations, causing indirect reductions in the amount of ammonium nitrate and ammonium sulfate in particulate matter. The magnitude of the impact on NH_3 and $PM_{2.5}$ concentrations exhibits a strong but non-linear dependence on the value of the uptake coefficient, with evidence for small but notable impacts on air quality even with the lowest assumed uptake coefficient of 10^{-5}.

1. Introduction

Atmospheric aerosols consist of inorganic species such as ammonium, nitrate, sulfate, water, chloride, elemental carbon, soil dust, and a wide variety of organic compounds. Fine particulate matter ($PM_{2.5}$) consists of approximately 25–50% inorganic compounds and 40–65% organic compounds on a mass basis (Gray et al., 1986; Zhang et al., 2000). Gaseous ammonia (NH_3) is a precursor to inorganic aerosols and is generally the limiting reactant in their formation (Wang et al., 2013; Lelieveld et al., 2015). Ammonium (NH_4^+) containing aerosols exhibit well-documented effects on climate (Adams et al., 2001; Martin et al., 2004; Abbatt et al., 2006; Henze et al., 2012) and health (Pope et al., 2002; Lelieveld et al., 2015). On the global scale, the largest sources of atmospheric NH_3 are agricultural activities and fertilizer use (Amann et al., 2013; Warner et al., 2017). Recent trends indicate that ambient NH_3 concentrations have been increasing over the last few decades and are expected to continue increasing in the future due in part to rising temperatures and expanding farming and animal husbandry operations (Amann et al., 2013; Warner et al., 2017).

In the South Coast Air Basin of California (SoCAB), a large fraction of total $PM_{2.5}$ mass is comprised of ammonium sulfate ((NH_4)$_2$$SO_4$) and ammonium nitrate ($NH_4NO_3$) (Kim et al., 2010). They are produced by the reaction of NH_3 with sulfuric acid (H_2SO_4) and nitric acid (HNO_3), respectively, and can cause adverse health effects and reduce visibility in the troposphere (US EPA, 2009). In the SoCAB, the largest NH_3 emission sources are agricultural activities (e.g., dairy facilities) and automobiles (Nowak et al., 2012), whereas HNO_3 and H_2SO_4 come from the oxidation of NO_x and SO_2 from various combustion sources. The total automobile and agricultural NH_3 emissions are estimated as similar in magnitude. However, the spatial concentration and high emissions of dairy facilities cause downwind NH_3 mixing ratios to be about an order of magnitude greater than those from vehicle emission sources (Nowak et al., 2012). These concentrated NH_3 plumes can be transported from their source region and react with inorganic acids to form ammonium salts. The high concentration of NH_3 in these plumes drives all of the H_2SO_4 and most of the HNO_3 into the particle phase, causing high concentrations of inorganic $PM_{2.5}$ in the northeast part of the SoCAB (Hughes et al., 2002; Neuman et al., 2003; Nowak et al., 2012).

The conversion of inorganic gases into ammonium, nitrate, and

* Corresponding author.
    E-mail address: ddabdub@uci.edu (D. Dabdub).

sulfate particles is now well understood. However, significant uncertainty remains regarding reactions between gaseous NH_3 and organic compounds found in secondary organic aerosols (SOA). Ammonia has been shown to react with certain carbonyl compounds found in SOA, as documented in a recent review on this topic (Laskin et al., 2015). These reactions convert NH_3 into heterocyclic nitrogen-containing organic compounds (NOC) that remain in particles. The neglect of this process may result in an incorrect prediction of the distribution of organics in PM, and at the same time, over-prediction of gas-phase NH_3, and therefore inorganic PM concentrations, in models. NOC have also been observed in ambient particles in California (O'Brien et al., 2013a, 2013b) and in China (Wang et al., 2010), with evidence for NH_3 playing a key role in their formation. For example, O'Brien et al. (2013b) analyzed the molecular composition of aerosol samples collected during CalNex 2010 in Bakersfield, California and concluded that NOC, which accounted for more than 40% of the observed organic compounds, were produced via reactions between NH_3 and carbonyl groups converting them into imines. Similarly, O'Brien et al. (2013a) compared the composition of field-collected and laboratory-generated SOA and found that some of the NOC observed in Bakersfield were likely formed through reactions of products of oxidation of diesel fuel emissions with gas-phase NH_3, potentially driven by high concentrations of gaseous NH_3 in the area. Their conclusions were supported by photochemical chamber experiments, where the addition of gaseous NH_3 to SOA generated from diesel fuel oxidation was necessary to produce many of the compounds observed in Bakersfield, and improved overlap between laboratory-generated and observed compounds. It is likely that similar reactions occur in the Los Angeles basin, particularly areas downwind of strong NH_3 emissions sources with high NH_3 concentrations.

In 2015, Liu et al. reported for the first time chemical uptake coefficients for NH_3 onto SOA particles measured by direct observation of NOC by an aerosol mass spectrometer (AMS). The initial uptake coefficients were on the order of 10^{-2} to 10^{-3}, dropping to 10^{-5} after six hours of reaction. Several other studies demonstrated chemical reactions between NH_3 and various types of SOA but have not quantified the uptake coefficients, rate constants, or equilibrium constants that could be used in models (Bones et al., 2010; Laskin et al., 2010; Updyke et al., 2012). The maximal yield of NOC in reactions between ammonia and SOA has not been quantified, but there are indications that the yield is modest, on the order of a few percent (Laskin et al., 2014).

In this exploratory study, a surface reaction between NH_3 and SOA particles is implemented into the University of California, Irvine – California Institute of Technology (UCI-CIT) model based on the NH_3 uptake coefficients onto SOA reported by Liu et al. (2015) to estimate the impact of this process on NH_3 and $PM_{2.5}$ concentrations. In addition, supplementary experiments are performed to better constrain the maximal possible fraction of NOC in SOA after long-term exposure to NH_3. Air quality simulations are conducted using a range of uptake coefficients to determine the sensitivity of NH_3 removal to the magnitude of the uptake coefficient. This study represents the first attempt to quantify the potential importance of including NH_3 + SOA chemistry in air quality models and presents the initial findings of implementing a simplified uptake mechanism into a high-resolution air quality model. Although there are limitations to the simplified mechanism implemented into the model, it provides a modeling framework and methodology that can be refined and applied in future studies to better characterize and simulate interactions between NH_3 and organic particles. In section 2, we describe the experimental and modeling methods used in this work, including the key assumptions used in the model calculations. In section 3, we present and discuss the results of the measurements and the air quality simulations, and in section 4, we discuss the need for air quality models to include this important process and present recommendations for future work.

2. Methodology

2.1. Experimental methods

In order to establish an upper limit on the fraction of SOA compounds that can be converted to NOC, we did several smog chamber experiments. SOA were synthesized in a $5\,m^3$ Teflon chamber by ozonolysis of limonene, low-NO_x oxidation of toluene and by low-NO_x oxidation of n-hexadecane at different values of relative humidity (see supporting information for details). Once sufficient particle mass concentration was produced, a ~200 ppb pulse of NH_3 was injected into the chamber. We deliberately used low-NO_x conditions (and no seed particles) to avoid interference between NOC formed during the oxidation and NOC resulting from the reactive uptake of NH_3 onto SOA particles. A time-of-flight aerosol mass spectrometer (ToF-AMS) was used to measure the O/C and N/C ratios in the SOA organics. Samples of SOA particles were collected onto Teflon filters and then exposed to NH_3 to achieve the maximal conversion of the initial SOA compounds into NOC. The filter exposure lasted for two days at an estimated NH_3 mixing ratio of 300 ppb. All the SOA samples were extracted subsequently with acetonitrile and analyzed via direct analysis in real time mass spectrometry (DART-MS). In order to avoid interference from inorganic salts in the DART-MS spectra, we deliberately did not use seed particles during SOA preparation.

2.2. Modeling methods

The UCI-CIT regional airshed model was used for the air quality simulations. The modeling domain covers the SoCAB, which contains Orange County and portions of Riverside, Los Angeles, San Bernardino, and Ventura counties (Fig. S1). It utilizes 994 computational cells, each with an area of $5\,km \times 5\,km$. The unique modeling domain encompasses a variety of landscapes, including seaside communities, urban and suburban areas, and agricultural activity centered around Chino. Numerous studies have used the UCI-CIT model to simulate air quality in the SoCAB (Nguyen and Dabdub, 2002; Carreras-Sospedra et al., 2006, 2010; Chang et al., 2010; Horne and Dabdub, 2017; Montoya-Aguilera et al., 2017). The model's chemical mechanism is based on the Caltech Atmospheric Chemical Mechanism (CACM) (Griffin et al., 2002a, 2002b, 2005), expanded to include additional SOA precursors (Dawson and Griffin, 2016). The 3-day episode August 27–29 is chosen for the air quality simulations, using meteorological conditions that typically occur in the region during the summertime and for which the model has been previously evaluated (Nguyen and Dabdub, 2002; Carreras-Sospedra et al., 2006, 2010; Chang et al., 2010), with 2008 emissions. The model's spatially and temporally resolved emissions are derived from the South Coast Air Quality Management District's 2012 Air Quality Management Plan (SCAQMD, 2013). A previous study conducted with the UCI-CIT model indicated that model-predicted NH_3 concentrations are similar to those measured in Chino during a field study (Perraud et al., 2015), supporting the accurate representation of NH_3 emissions in the model. Initial conditions and boundary conditions are based on values typical to the region. All results presented in this study are from the final simulation day using the emissions described above.

To explore the potential impact of the heterogeneous uptake of NH_3 by SOA on air quality, a parameterization of the removal of gaseous NH_3 by SOA compounds was implemented into the UCI-CIT model as follows. First, the total concentration of SOA in each of the eight size bins ($Cmass_1$, $Cmass_2$, …, $Cmass_8$) was calculated. Next, assuming spherical particles with a density of $1.2\,g/cm^3$, the area of SOA particles per volume of air was computed for each size bin ($Carea_1$, $Carea_2$, …, $Carea_8$) from the mass concentration of SOA in each bin ($Cmass_1$, $Cmass_2$, …, $Cmass_8$) and the representative (average) diameter of particles in that bin (dp_1, dp_2, …, dp_8).

$$C_{area_i} = \frac{C_{mass_i}}{\rho} \times \frac{6}{d_{p_i}}$$

The total available area of SOA particles per volume of air was then determined by summing the combined area of SOA particles in each of the eight size bins.

$$C_{area} = \sum_{i=1}^{8} area_i$$

The area calculated by this approach is an approximation for the surface area presented by the SOA compounds because the actual particles contain inorganic species and have complex non-spherical morphologies. Finally, using an average speed of NH_3 molecules of 6.1×10^2 m/s (v_{NH_3}) at 298 K, the first-order loss rate constant, k, was calculated as

$$k = \gamma \times \frac{v_{NH_3} \times C_{area}}{4}$$

where γ is the reactive uptake coefficient for NH_3. The above calculations were performed separately for each model grid cell at every time step to determine the effective first order rate constant in that cell at that time. The loss rate for NH_3 was then determined from the first-order rate constant and the gas-phase NH_3 concentration in that cell at that time, with one limitation. The loss rate for NH_3 was limited by the yield of NOC observed in previous studies (Laskin et al., 2014) and estimated in this work (see below). Specifically, we assumed that the yield of NOC from reactions between NH_3 and SOA compounds cannot exceed 10%. Therefore, the maximum amount of NH_3 that can be taken up by SOA in each model grid cell at each time step is 0.1 mole of NH_3 per mole of SOA compounds.

Ammonia uptake coefficients (γ values) were obtained from Liu et al. (2015), who studied particulate NOC formation after SOA formed from OH oxidation of *m*-xylene and ozonolysis of α-pinene were exposed to NH_3. They showed that NOC compounds can be formed reasonably quickly via the uptake of NH_3 by SOA and reported uptake coefficients for NH_3 onto SOA ranging from 10^{-5} to 10^{-2}, with an average value of 4.0×10^{-3}. Here, simulations were performed with a variety of γ values as reported by Liu et al. (2015) to determine the sensitivity of NH_3 removal to changes in the uptake coefficient. In total, five scenarios were considered: (a) reference case with no NH_3 uptake, (b) NH_3 uptake with $\gamma = 10^{-2}$, (c) NH_3 uptake with $\gamma = 10^{-3}$, (d) NH_3 uptake with $\gamma = 10^{-4}$, and (e) NH_3 uptake with $\gamma = 10^{-5}$. Results for (b), (c), (d), and (e) were compared to the reference case model simulations in (a), where the removal of NH_3 by SOA was not included, to determine the impact on NH_3 and $PM_{2.5}$ concentrations. This study assumes that γ remains constant in each scenario (i.e., no saturation effects) and therefore each scenario represents an upper limit to the amount of NH_3 removed by SOA with the selected uptake coefficient. However, the uptake is programmed to stop once the molar fraction of NOC in SOA particles reaches 0.1, as mentioned above. A sensitivity analysis was performed to determine the influence of this assumption on simulation results. Additional model runs conducted assuming a maximum NOC molar fraction of 0.05 or 0.20 changed domain-averaged NH_3 and $PM_{2.5}$ concentrations by < 1% in all scenarios except (b) when the largest uptake coefficient (10^{-2}) is utilized. Although the impact on gas-phase NH_3 concentrations in this scenario is reduced and increased by about 5% when changing the assumed molar fraction of NOC from 0.10 to 0.05 and from 0.10 to 0.20, respectively, the impact on $PM_{2.5}$ concentrations remains essentially unchanged in both cases. All other model inputs (emissions, meteorology, etc.) are held constant between each scenario. Results presented here are for the final simulation day to provide adequate time for NH_3 uptake processes to occur and minimize the influence of initial conditions.

This study assumes that the NOC products of reactions between NH_3 and particulate organics remain in the particles and do not cause a significant increase in the mass concentration of particulate organics. In

these reactions, carbonyl groups are first converted into primary imines, and further reactions lead to more stable secondary imines and heterocyclic compounds (Laskin et al., 2015). The uptake of NH_3 is accompanied by loss of one or several water molecules, and the molecular weight and volatility of the NOC product should not be too different from those of the starting SOA compound. Indeed, experiments by Liu et al. (2015) and experiments described in the supplementary material show that there is no significant change in the particle mass concentration after exposure of SOA particles to NH_3. Furthermore, although reactions between NH_3 and organic acids/carbonyls can potentially lead to condensable NOC (Duporté et al., 2017), we assume that the contribution of these reactions to particle-phase NOC is negligible based on the results of Liu et al. (2015). In Liu et al. (2015), gas-phase reactions leading to particulate NOC were assumed to be negligible based on (1) the observed anti-correlation between the calculated reactive uptake coefficient and NH_3 concentration, and (2) the exceedingly slow rate of the termolecular reaction between NH_3, acid, and carbonyls required in the gas phase to form particle-phase NOC. Therefore, the chemical uptake of gas-phase NH_3 in the model is assumed to occur only via the surface reaction with SOA particles.

This study also assumes that NOC are less effective than NH_3 in neutralizing inorganic acids. In other words, the formation of nitrates and sulfates of protonated NOC (salts containing an organic cation and inorganic anion) is neglected. If the basicity of NOC were as high as that of NH_3, the conversion of NH_3 into NOC would cause little to no change in PM concentrations. However, NH_3 is a stronger base compared to the stable NOC products it forms: the $pK_b = 4.8$ of NH_3 is smaller than pK_b of secondary imines ($pK_b \sim 10$) and nitrogen containing aromatic compounds (e.g., pyrrole $pK_b = 13.6$, pyridine $pK_b = 8.8$). Therefore, neglect of NOC salts is a reasonable approximation.

3. Results and discussion

3.1. Experimental observations

After exposure of SOA to a pulse of NH_3 in the chamber, there was no change in the particle mass concentration for any of the three SOA systems (Fig. S2). After the experiments, we were able to get an NH_3 analyzer, which showed that most of the injected NH_3 was actually quickly removed by the chamber walls making it impossible for us to quantify the uptake coefficient from the ToF-AMS data. Despite the NH_3 wall loss, slow chemical uptake of NH_3 was observable in some ToF-AMS data. Specifically, when limonene/O_3 SOA was exposed to NH_3, there was a slow increase in the N:C ratio (Fig. S3). However, we observed no uptake of NH_3 on toluene/OH SOA (Fig. S3), despite the fact that efficient uptake was observed by Liu et al. (2015) for related xylene/OH SOA. It is possible that the difference is due to the presence of NO_x in Liu et al. experiments and absence of NO_x in our experiments; the presence of nitric acid produced by photooxidation of NO_x is likely to promote uptake of NH_3 and subsequent acid-catalyzed conversion of NH_3 to NOC.

There was an increase in the abundance of even *m/z* peaks in the DART mass spectra of the limonene/O_3 SOA particles that were exposed to NH_3 in the chamber (Fig. S4). The fraction of NOC ($f_N = 20\%$) was estimated from the increases in the relative abundance of the even *m/z* peaks in the DART mass spectra based on the procedure described in the supporting information section. Liu et al. (2015) reported comparable conversion efficiencies for SOA particles, with 9% of α-pinene/O_3 SOA compounds and 32% of m-xylene SOA compounds (by mass) being converted to NOC. Prolonged exposure of bulk SOA filter samples to NH_3 led to browning of limonene/O_3 SOA material, as observed in previous experiments (Updyke et al., 2012). The limonene/O_3 bulk SOA sample exposed to NH_3 on a filter had an f_N value of 11%, lower than that resulting from an exposure of SOA particles to NH_3 in the chamber. These results suggest that NH_3 reacts with SOA more efficiently with suspended particles compared to the bulk SOA sample. The f_N values for
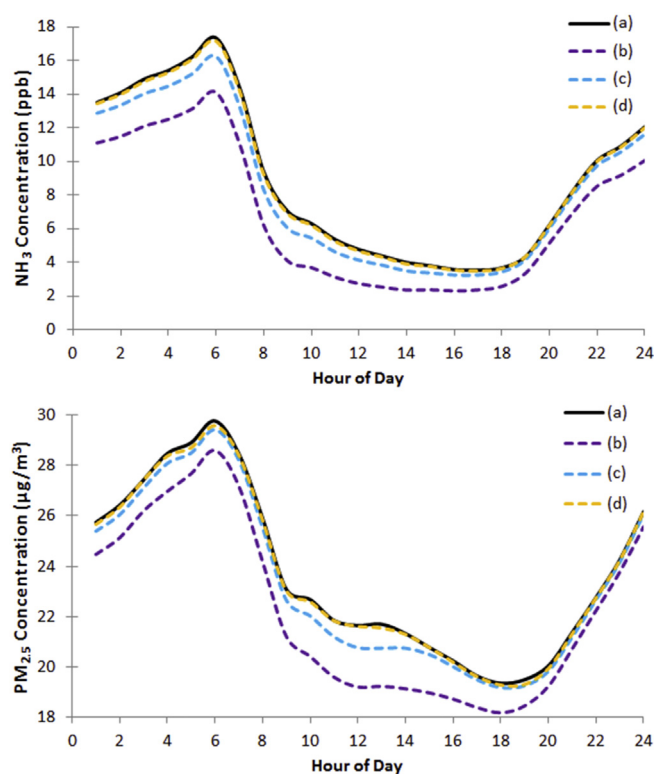
Fig. 1. Domain wide average concentrations of ammonia (NH$_3$, top panel) and PM$_{2.5}$ (bottom panel) in the (a) base case, (b) $\gamma = 10^{-2}$ scenario, (c) $\gamma = 10^{-3}$ scenario, and (d) $\gamma = 10^{-4}$ scenario. Ammonia and PM$_{2.5}$ concentrations change by less than 1% at all hours of the day in the $\gamma = 10^{-5}$ scenario (not shown).

the toluene/OH and hexadecane/OH bulk SOA samples exposed to NH$_3$ were a factor of two smaller than for limonene/O$_3$ SOA, with an f$_N$ of 5% for both samples. This suggests that different types of SOA exhibit different reactivity towards NH$_3$. The low values of f$_N$ observed in this work are similar to the results of Laskin et al. (2014), who estimated from IR spectra that less than 5% of SOA carbonyls in SOA filter samples are converted in NOC.

In summary, the experiments described here generally support the assumptions made in the model, specifically, the assumption that on the order of 10% of SOA compounds can be converted to NOC. However, they do not provide additional information on the uptake coefficients relative to the previous study by Liu et al. (2015).

3.2. Model predictions

The air quality impacts of including the uptake of NH$_3$ by SOA vary greatly between scenarios depending on the magnitude of the uptake coefficient. Table S1 and Fig. 1 show the impact of the NH$_3$ + SOA reactions on the domain-averaged hourly NH$_3$ and PM$_{2.5}$ concentrations. When using $\gamma = 10^{-2}$, domain wide average NH$_3$ concentrations decrease by 15–40%, with the greatest percentage decreases (30–40%) occurring between 08:00 h and 17:00 h local time. Because domain wide averages are computed by averaging all cells in the model domain, this indicates that more than one third of all gas-phase NH$_3$ in the basin is removed in this scenario during these times. However, the decrease in NH$_3$ concentrations is highly spatially dependent. In certain areas, such as those with a high concentration of SOA and relatively low (< 40 ppb) gas-phase NH$_3$ concentrations in the reference case, hourly NH$_3$ concentrations decrease by over 60%. On the other hand, areas near the coast experience little change in NH$_3$ concentration due to low levels of both gaseous NH$_3$ and SOA in the reference case (see Fig. S7

for map of SOA concentrations in the reference case).

Fig. 2 shows the spatially resolved 24-h average NH$_3$ concentrations in the reference case and the changes induced by the reactive uptake of NH$_3$. The greatest decreases occur near and downwind of areas with agricultural activity and large quantities of NH$_3$ emissions. 24-hour average NH$_3$ concentrations near Chino peak at 250 ppb in the reference case, and are reduced by up to 15 ppb in the same area when using $\gamma = 10^{-2}$ (Fig. 2b, left column). Although the greatest decreases occur near the strongest emissions sources, NH$_3$ continues to be removed by SOA as it is transported further inland. As a result, hourly and 24-h average NH$_3$ concentrations decrease by 15–20 ppb and 5–10 ppb, respectively, for many areas in the northeast portion of the basin. Changes in the concentration of gas-phase NH$_3$ can affect the formation of inorganic PM due to its rapid reaction with different acids (e.g., nitric and sulfuric) to form corresponding salts, which contribute to secondary particle formation and particle growth (Schiferl et al., 2014).

Table S1 shows domain-averaged concentrations of PM$_{2.5}$ in the reference case, as well as the absolute and percent change in concentration for scenarios (b), (c), and (d) versus the reference case, (a). With the uptake coefficient of 10^{-2} used in this scenario, decreases in domain wide average concentrations range from 2% late at night to 11% during midday (Fig. 1). In some locations, the impact on hourly PM$_{2.5}$ concentrations is far greater, with decreases up to 35 μg/m^3 (60%) in areas northeast of Riverside. A combination of meteorological and geographical features in the SoCAB cause the buildup of pollutants in the downwind (northeastern) portion of the basin. A sea breeze during the daytime hours causes predominantly southwesterly winds while the northern edge of the domain is bounded by mountainous terrain in the Angeles and San Bernardino National Forests, preventing pollutants from being transported further inland. Thus, NH$_3$ continues to be taken up by SOA as it is transported inland, causing the largest impacts on PM to occur in the downwind areas of the basin where a variety of anthropogenic and biogenic precursors accumulate, rather than near NH$_3$ emissions sources.

Fig. 2 shows that the greatest impacts on 24-h average PM$_{2.5}$ concentrations occur in the northeastern area of the basin. Here, reference case levels range from 40 to 55 μg/m^3 (Fig. 2), and decrease by up to 15 μg/m^3 in this scenario (Fig. 2b, right column). Previous studies showed that concentrated NH$_3$ plumes from agricultural activity shift the NH$_4$NO$_3$ equilibrium towards the particle phase, leading to coincident formation of NO$_3^-$ and NH$_4^+$ particles and depletion of gas-phase HNO$_3$ in downwind areas of the basin (Hughes et al., 2002; Neuman et al., 2003; Nowak et al., 2012). Additionally, these studies suggested that NH$_4$NO$_3$ particle formation in the SoCAB could be best controlled by reducing the highly concentrated NH$_3$ emissions from agricultural activity, rather than emissions from automobiles, which are well distributed throughout the domain. Here we show that decreases in NH$_3$ concentration due to uptake by SOA reduce the availability of gas-phase NH$_3$ to react with HNO$_3$ and H$_2$SO$_4$ to form NH$_3$ nitrate and ammonium sulfate particles, and that the largest impacts occur directly downwind of strong NH$_3$ emissions sources. Changes in the concentration of gas-phase HNO$_3$ and H$_2$SO$_4$, shown in Fig. S4, are consistent with this result. Because gas-phase HNO$_3$ and H$_2$SO$_4$ concentrations are inversely correlated with gas-phase NH$_3$ concentrations, HNO$_3$ and H$_2$SO$_4$ concentrations are generally higher in scenarios (b), (c), (d) and (e) than in the reference case. In particular, areas that show decreases in ammonium nitrate particle concentrations typically show increases in gas-phase nitric acid concentrations. This confirms that reductions in gas-phase NH$_3$ concentrations cause the equilibrium between NH$_3$(g) and NH$_4$NO$_3$(s) to shift toward the gas phase.

Fig. 3 shows reference case levels and the change in 24-h nitrate (NO$_3^-$), ammonium (NH$_4^+$), and sulfate (SO$_4^{2-}$) particle concentrations for scenarios (b), (c), (d) and (e) versus the reference case, (a). These figures show that although the spatial distribution of these species differs in the reference case (because of the different patterns of SO$_2$ and NO$_x$ emissions), the largest changes in 24-h average
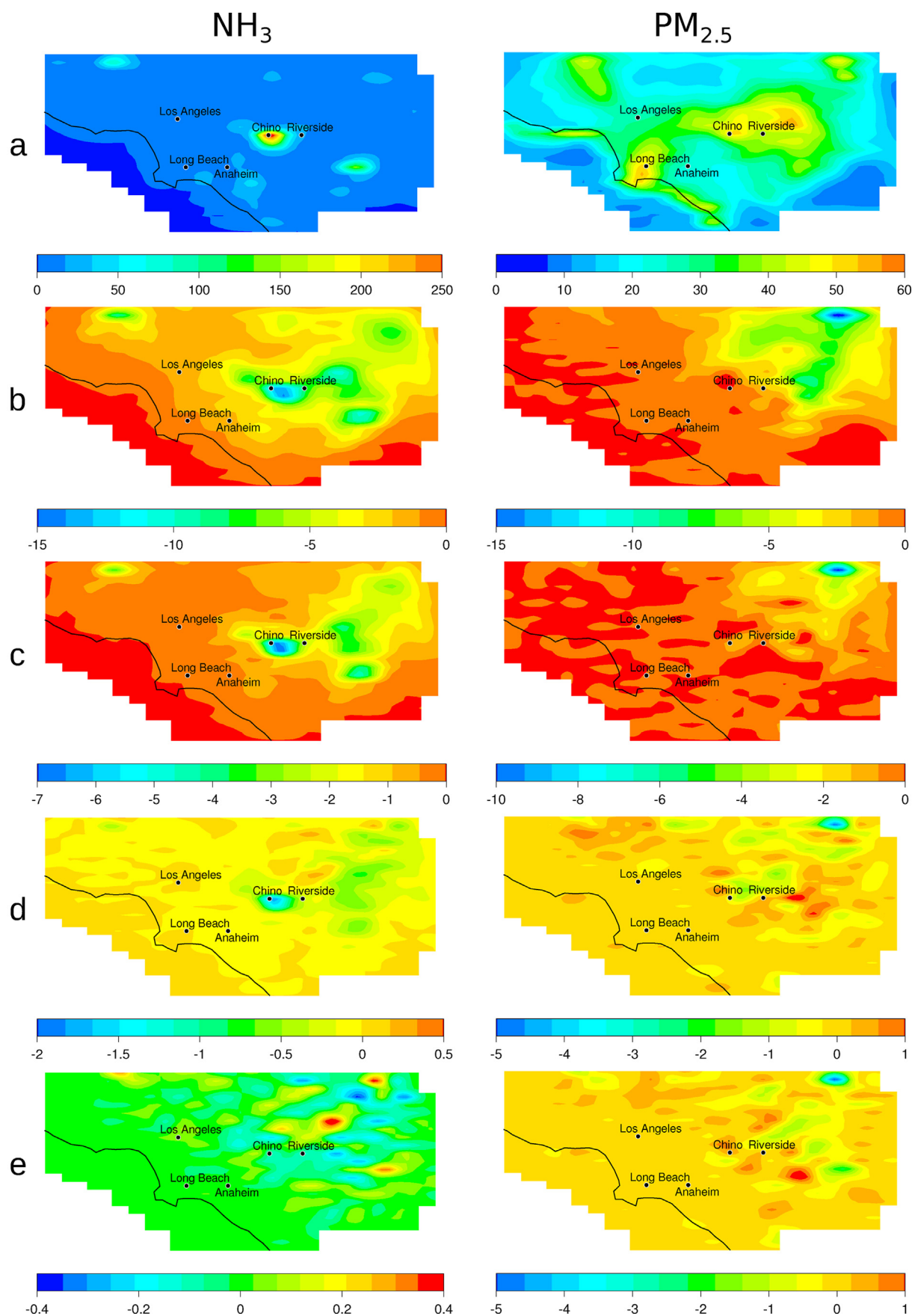
Fig. 2. 24-hour average concentrations of NH_3 (ppb) and $PM_{2.5}$ ($\mu g/m^3$) in the reference case shown in (a). Difference in concentration versus the reference case shown in rows (b), (c), (d), and (e) when using (b) $\gamma = 10^{-2}$, (c) $\gamma = 10^{-3}$, (d) $\gamma = 10^{-4}$, and (e) $\gamma = 10^{-5}$. Concentration decreases relative to the reference case are indicated by negative values.
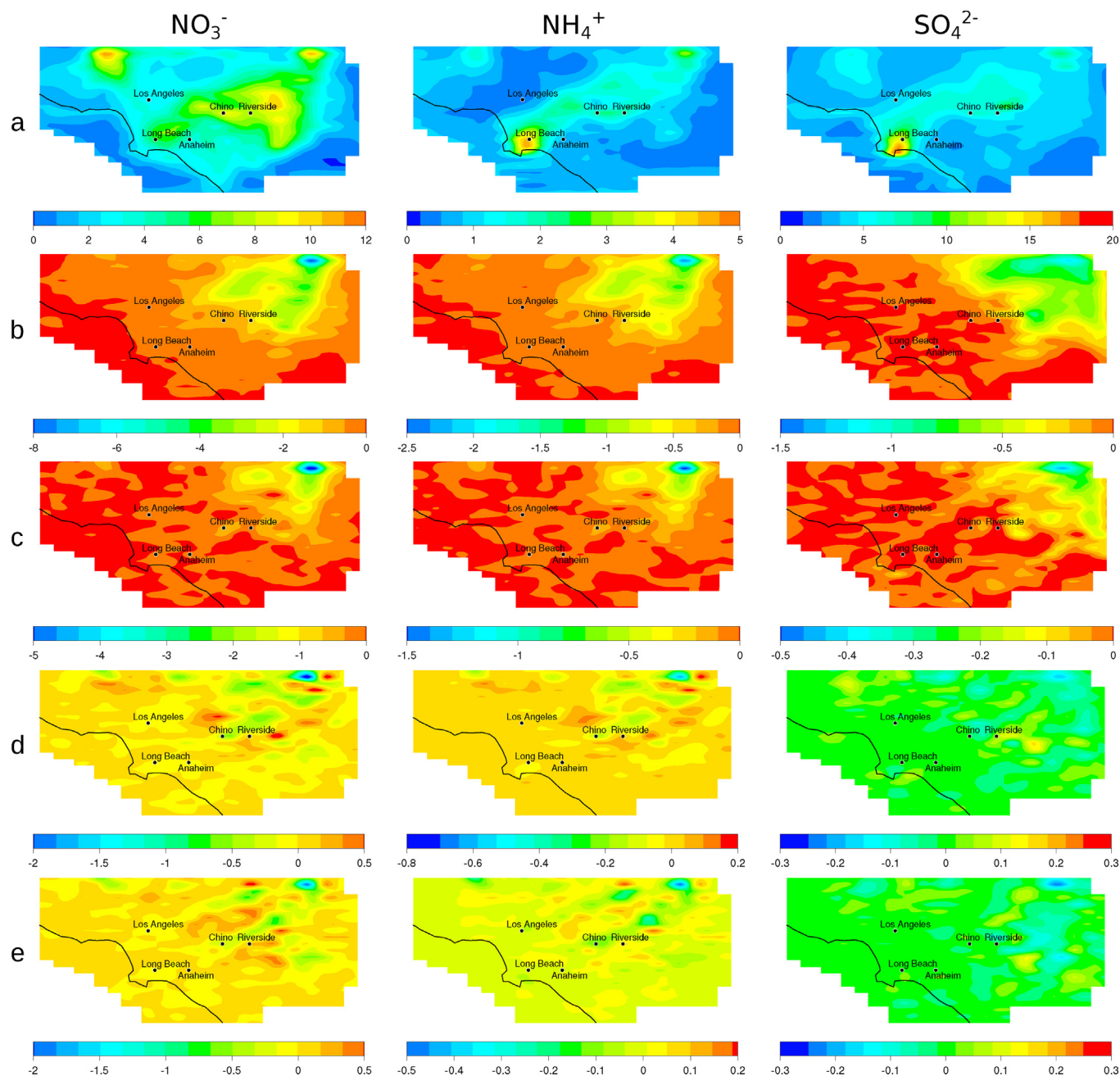
Fig. 3. 24-h average concentrations of particulate nitrate (NO_3^-, µg/m³), ammonium (NH_4^+, µg/m³) and sulfate (SO_4^{2-}, µg/m³) in the base case shown in (a). Difference in concentration versus the base case shown in rows (b), (c), (d) and (e) when using (b) $\gamma = 10^{-2}$, (c) $\gamma = 10^{-3}$, (d) $\gamma = 10^{-4}$ and (e) $\gamma = 10^{-5}$. Concentration decreases relative to the reference case are indicated by negative values.

concentrations for all three particulate species generally occur in the same geographical area northeast of Riverside. Together, decreases in nitrate, ammonium, and sulfate particle concentrations account for essentially all of the decrease in total $PM_{2.5}$ concentrations shown in Fig. 2. The spatial distribution and magnitude of model-predicted nitrate particle concentrations in the reference case (Fig. 3a, left column) agree with those measured by Neuman et al. (2003), who reported a peak concentration of 12.7 µg/m³ near Rubidoux.

In scenario (c), when the uptake coefficient is set to 10^{-3}, the magnitude of the impact on NH_3 and $PM_{2.5}$ concentrations is lower than in scenario (b), although the spatial distribution of changes remains similar. In this case, hourly domain wide average NH_3 concentrations decrease by 3–14% (Table S1), with some locations experiencing decreases of over 25% compared to reference case levels. Fig. 2c (left

column) shows that the largest impacts on gas-phase NH_3 occur in the same areas as in scenario (b), with decreases in 24-h average concentrations of about 7 ppb near Chino where the strongest NH_3 emissions sources in the basin are located. Although 24-h average NH_3 concentrations decrease by only 2–4 ppb in areas downwind of Riverside, the spatial distribution of changes in total $PM_{2.5}$ (Fig. 2, right column), as well as in nitrate, ammonium, and sulfate particle concentrations (Fig. 3) is similar in scenarios (b) and (c). In both scenarios, the largest reductions in 24-h average particle concentrations occur northeast of Riverside. Comparing parts (b) and (c) of Figs. 2 and 3 illustrates this result. Although the impact is lower than in scenario (b) due to the uptake coefficient being reduced by an order of magnitude, significant reductions in $PM_{2.5}$ concentrations still occur in this scenario. Decreases in 24-h average concentrations of 2–4 µg/m³ cover

large areas in the northeast portion of the basin, with peak decreases reaching $10 \, \mu g/m^3$. Given that the national standard for 24-h average $PM_{2.5}$ concentrations is $35 \, \mu g/m^3$, decreases of this magnitude have important implications for reaching attainment of national ambient air quality stands for fine particulate matter. Reducing 24-h average gas-phase NH_3 concentrations by only a few ppb significantly reduces the formation of ammonium nitrate and ammonium sulfate particles. Similar to scenario (b), the impact on hourly $PM_{2.5}$ concentrations is even greater, with decreases exceeding $20 \, \mu g/m^3$ (33%) in downwind areas of the basin during the afternoon hours. Coastal areas and locations upwind of NH_3 emissions sources again experience little to no change in NH_3 or $PM_{2.5}$ concentrations.

In scenario (d) with $\gamma = 10^{-4}$, domain wide average NH_3 concentrations decrease by only a few percent at all hours of the day (Table S1). Although isolated locations in the basin experience larger decreases, the overall impact on NH_3 concentrations is small when an uptake coefficient of 10^{-4} is used. Decreases in 24-h average NH_3 concentrations peak at 2 ppb and show a similar spatial distribution to those seen in scenario (c) (Fig. 2, left column). Areas downwind of strong emissions sources show decreases of 0.5–1 ppb, causing 24-h average $PM_{2.5}$ concentrations to decrease by $1–5 \, \mu g/m^3$. This indicates that the formation of ammonium nitrate and ammonium sulfate particles in the SoCAB is highly sensitive to changes in gas-phase NH_3 concentrations, consistent with Schiferl et al. (2014). The largest decreases in $PM_{2.5}$ concentrations again occur in the far northeast portion of the basin where pollutants accumulate. Peak decreases in hourly $PM_{2.5}$ concentrations reach $12 \, \mu g/m^3$ (20%) in some locations, although decreases of this magnitude are localized to highly impacted areas and only occur at certain times of the day. Overall, the impact on 24-h average NH_3 and $PM_{2.5}$ concentrations is around a factor of 2–3 lower in this scenario than scenario (c).

In the final scenario (e), an uptake coefficient of 10^{-5} is utilized. Although this uptake coefficient is three orders of magnitude lower than that used in scenario (b), peak decreases in $PM_{2.5}$ concentrations are only a factor of three lower. However, decreases of this magnitude are isolated to only a small area in the northeast corner of the basin. There are only small changes in NH_3 concentrations in this scenario. Hourly domain wide average NH_3 concentrations change by less than 1%, and most individual locations show decreases of only a few percent. Changes in 24-h average NH_3 concentrations are less than 0.5 ppb, as shown in Fig. 2e (left column). In contrast to scenarios (b) and (c), the increases and decreases in NH_3 concentrations are similar in magnitude in this scenario. Additionally, changes in NH_3 concentrations in this scenario are less localized and occur throughout the inland portion of the basin. Reducing the magnitude of the uptake coefficient increases the lifetime of NH_3, causing the spatial distribution of impacts to be more dependent on the meteorological conditions in the basin during the first two days and into day three. Fig. 2 (right column) shows that the spatial distribution of changes in $PM_{2.5}$ concentrations is also different in this scenario than in scenarios (b) and (c). Here, changes in 24-h average $PM_{2.5}$ levels of $\pm 1 \, \mu g/m^3$ occur at various locations, with decreases of $1–2 \, \mu g/m^3$ occurring in downwind areas of the basin. However, domain wide average $PM_{2.5}$ concentrations decrease by less than 1% at all hours of the day, indicating that the overall impact on fine particle concentrations is small. As in the previous scenarios, changes in the concentration of ammonium and nitrate particles cause nearly all of the change in total $PM_{2.5}$ concentrations. Overall, the impact on both gas-phase and particulate species is of variable sign when the lowest uptake coefficient of 10^{-5} is utilized.

4. Conclusions and future directions

Our results indicate that the chemical uptake of NH_3 by SOA can reduce the concentration of gas-phase NH_3, thereby reducing the potential to form ammonium nitrate and ammonium sulfate in the particle phase. The main chemical mechanism for this is the conversion of NH_3

in SOA particles to less basic nitrogen-containing organic compounds that are less efficient in neutralizing inorganic acids than NH_3 is. We show that the inclusion of this previously unaccounted for sink for gas-phase NH_3 into an urban airshed model reduces 24-h average $PM_{2.5}$ concentrations by up to $15 \, \mu g/m^3$ in highly impacted areas. However, this result should be seen as an upper limit as it reflects the use of the largest plausible uptake coefficient (10^{-2}) without any consideration of possible reaction saturation effects. It is more likely that the changes in $PM_{2.5}$ concentrations caused by the uptake of NH_3 by SOA are in the $1–5 \, \mu g/m^3$ range, as projected in scenarios (d) and (e). Results also indicate that the formation of inorganic $PM_{2.5}$ is highly sensitive to changes in the concentration of gas-phase NH_3, as reductions in 24-h average NH_3 concentrations of 0.5–2 ppb cause 24-h average $PM_{2.5}$ concentrations to decrease by $1–5 \, \mu g/m^3$ in downwind areas (see Fig. 2d). Previous studies have shown that ammonium nitrate particles form when concentrated NH_3 plumes are mixed into areas of active urban photochemistry, such as the northeast portion of the SoCAB (Nowak et al., 2012; Schiferl et al., 2014). Both primary and secondary pollutants accumulate in the northeast portion of the basin, which is photochemically active and where high temperatures are observed during the summer months. Thus, while the largest decreases in gas-phase NH_3 concentrations occur near the strongest emissions sources, the largest decreases in $PM_{2.5}$ concentrations occur in downwind areas, particularly northeast of Riverside. Together, changes in the concentration of nitrate, ammonium, and sulfate particles account for essentially all of the decrease in total $PM_{2.5}$ concentrations.

Our study presents the initial findings of including this previously unaccounted for process in air quality models. Because inorganic particles (comprised of ammonium, sulfate and nitrate) represent a large portion of total fine particulate matter mass in the SoCAB (Kim et al., 2010; Schiferl et al., 2014) and many other locations around the world, accurate modeling of gas-phase NH_3 concentrations is essential for predicting future air quality. Although we focus on the South Coast Air Basin of California, results shown here have important global implications as NH_3 emissions have shown increasing trends over the last few decades and are expected to increase even more in the future (Amann et al., 2013; Warner et al., 2017). Models used to simulate air quality and climate should take into account the uptake of NH_3 by SOA, which is especially important in agricultural areas with strong NH_3 emissions sources. Additionally, models used in the development of air quality management strategies should account for changes in the concentration of NH_3 due to its uptake by SOA to ensure accurate prediction of $PM_{2.5}$ concentrations. Because significant uncertainty remains regarding the mechanism, rate and extent of reactions between gaseous NH_3 and organic compounds found in SOA, additional studies are needed to better constrain and quantify uptake coefficients for a variety of SOA compounds. Future studies should also account for changes in the chemical composition of SOA due to its uptake of NH_3 as additional results from laboratory experiments and field studies become available.

Appendix A. Supplementary data

Supplementary data related to this article can be found at http://dx.doi.org/10.1016/j.atmosenv.2018.06.021.

References

Abbatt, J.P.D., Benz, S., Cziczo, D.J., Kanji, Z., Lohmann, U., Mohler, O., 2006. Solid ammonium sulphate aerosols as ice nuclei: a pathway for cirrus cloud formation. Science 313, 1770. http://dx.doi.org/10.1126/science1129726.

Adams, P.J., Seinfeld, J.H., Koch, D., Mickley, L., Jacob, D., 2001. General circulation model assessment of direct radiative forcing by the sulfate–nitrate–ammonium–water inorganic aerosol system. J. Geophys. Res. 106, 1097–1111. http://dx.doi.org/10.1029/2000JD900512.

Amann, M., Klimont, Z., Wagner, F., 2013. Regional and global emissions of air pollutants: recent trends and future scenarios. Annu. Rev. Environ. Resour. 38, 31–55.

Bones, D.L., Henricksen, D.K., Mang, S.A., Gonsior, M., Bateman, A.P., Nguyen, T.B., Cooper, W.J., Nizkorodov, S.A., 2010. Appearance of strong absorbers and fluorophores in limonene-O₃ secondary organic aerosol due to NH₄⁺-mediated chemical aging over long time scales. J. Geophys. Res.: Atmosphere 115 (D5).

Carreras-Sospedra, M., Dabdub, D., Rodriguez, M., Brouwer, J., 2006. Air quality modeling in the South Coast Air Basin of California: what do the numbers really mean? J. Air Waste Manag. Assoc. 56 (8), 1184–1195.

Carreras-Sospedra, M., Vutukuru, S., Brouwer, J., Dabdub, D., 2010. Central power generation versus distributed generation–An air quality assessment in the South Coast Air Basin of California. Atmos. Environ. 44 (26), 3215–3223.

Chang, W.L., Griffin, R.J., Dabdub, D., 2010. Partitioning phase preference for secondary organic aerosol in an urban atmosphere. Proc. Natl. Acad. Sci. Unit. States Am. 107 (15), 6705–6710.

Dawson, M.L., Griffin, R.J., 2016. Development of aroCACM/MPMPO 1.0: a model to simulate secondary organic aerosol from aromatic precursors in regional models. Geosci. Model Dev. (GMD) 9 (6), 2143.

Duporté, G., Riva, M., Parshintsev, J., Heikkinen, E., Barreira, L.M., Myllys, N., Heikkinen, L., Hartonen, K., Kulmala, M., Ehn, M., Riekkola, M.L., 2017. Chemical characterization of gas-and particle-phase products from the ozonolysis of α-pinene in the presence of dimethylamine. Environ. Sci. Technol. 51 (10), 5602–5610. http://dx.doi.org/10.1021/acs.est.6b06231.

Gray, H.A., Cass, G.R., Huntzicker, J.J., Heyerdahl, E.K., Rau, J.A., 1986. Characteristics of atmospheric organic and elemental carbon particle concentrations in Los Angeles. Environ. Sci. Technol. 20 (6), 580–589.

Griffin, R.J., Dabdub, D., Seinfeld, J.H., 2002a. Secondary organic aerosol 1. Atmospheric chemical mechanism for production of molecular constituents. J. Geophys. Res.: Atmosphere 107 (D17), 107. http://dx.doi.org/10.1029/2001JD000541.

Griffin, R.J., Dabdub, D., Kleeman, M.J., Fraser, M.P., Cass, G.R., Seinfeld, J.H., 2002b. Secondary organic aerosol 3. Urban/regional scale model of size-and composition-resolved aerosols. J. Geophys. Res.: Atmosphere 107 (D17), 4334. http://dx.doi.org/10.1029/2001JD000544.

Griffin, R.J., Dabdub, D., Seinfeld, J.H., 2005. Development and initial evaluation of a dynamic species-resolved model for gas phase chemistry and size-resolved gas/particle partitioning associated with secondary organic aerosol formation. J. Geophys. Res.: Atmosphere 110, D05304. http://dx.doi.org/10.1029/2004JD005219.

Henze, D.K., Shindell, D.T., Akhtar, F., Spurr, R.J.D., Pinder, R.W., Loughlin, D., Kopacz, M., Sing, K., Shim, C., 2012. Spatially refined aerosol direct radiative forcing efficiencies. Environ. Sci. Technol. 46 (17), 9511–9518. http://dx.doi.org/10.1021/es301993s.

Horne, J.R., Dabdub, D., 2017. Impact of global climate change on ozone, particulate matter, and secondary organic aerosol concentrations in California: a model perturbation analysis. Atmos. Environ. 153, 1–17.

Hughes, L.S., Allen, J.O., Salmon, L.G., Mayo, P.R., Johnson, R.J., Cass, G.R., 2002. Evolution of nitrogen species air pollutants along trajectories crossing the Los Angeles area. Environ. Sci. Technol. 36 (18), 3928–3935.

Kim, E., Turkiewicz, K., Zulawnick, S.A., Magliano, K.L., 2010. Sources of fine particles in the South Coast area, California. Atmos. Environ. 44 (26), 3095–3100.

Laskin, J., Laskin, A., Roach, P.J., Slysz, G.W., Anderson, G.A., Nizkorodov, S.A., Bones, D.L., Nguyen, L.Q., 2010. High-resolution desorption electrospray ionization mass spectrometry for chemical characterization of organic aerosols. Anal. Chem. 82 (5), 2048–2058.

Laskin, J., Laskin, A., Nizkorodov, S.A., Roach, P., Eckert, P., Gilles, M.K., Wang, B., Lee, H.J., Hu, Q., 2014. Molecular selectivity of brown carbon chromophores. Environ. Sci. Technol. 48 (20), 12047–12055.

Laskin, A., Laskin, J., Nizkorodov, S.A., 2015. Chemistry of atmospheric brown carbon. Chem. Rev. 115 (10), 4335–4382. http://dx.doi.org/10.1021/cr5006167.

Lelieveld, J., Evans, J.S., Fnais, M., Giannadaki, D., Pozzer, A., 2015. The contribution of outdoor air pollution sources to premature mortality on a global scale. Nature 525 (7569), 367–371.

Liu, Y., Liggio, J., Staebler, R., Li, S.M., 2015. Reactive uptake of ammonia to secondary organic aerosols: kinetics of organonitrogen formation. Atmos. Chem. Phys. 15 (23), 13569–13584. http://dx.doi.org/10.5194/acp-15-13569-2015.

Martin, S.T., Hung, H.M., Park, R.J., Jacob, D.J., Spurr, R.J.D., Chance, K.V., Chin, M., 2004. Effects of the physical state of tropospheric ammonium-sulfate-nitrate particles on global aerosol direct radiative forcing. Atmos. Chem. Phys. 4 (1), 183–214. http://dx.doi.org/10.5194/acp-4-183-2004.

Montoya-Aguilera, J., Horne, J.R., Hinks, M.L., Fleming, L.T., Perraud, V., Lin, P., Laskin, A., Laskin, J., Dabdub, D., Nizkorodov, S.A., 2017. Secondary organic aerosol from atmospheric photooxidation of indole. Atmos. Chem. Phys. 17, 11605–11621. https://doi.org/10.5194/acp-17-11605-2017.

Neuman, J.A., Nowak, J.B., Brock, C.A., Trainer, M., Fehsenfeld, F.C., Holloway, J.S., Hübler, G., Hudson, P.K., Murphy, D.M., Nicks, D.K., Orsini, D., 2003. Variability in ammonium nitrate formation and nitric acid depletion with altitude and location over California. J. Geophys. Res.: Atmosphere 108 (D17). http://dx.doi.org/10.1029/2003JD003616.

Nguyen, K., Dabdub, D., 2002. NOx and VOC control and its effects on the formation of aerosols. Aerosol Sci. Technol. 36 (5), 560–572.

Nowak, J.B., Neuman, J.A., Bahreini, R., Middlebrook, A.M., Holloway, J.S., McKeen, S.A., Parrish, D.D., Ryerson, T.B., Trainer, M., 2012. Ammonia sources in the California South Coast Air Basin and their impact on ammonium nitrate formation. Geophys. Res. Lett. 39 (7). http://dx.doi.org/10.1029/2012GL051197.

O'Brien, R.E., Nguyen, T.B., Laskin, A., Laskin, J., Hayes, P.L., Liu, S., Jimenez, J.L., Russell, L.M., Nizkorodov, S.A., Goldstein, A.H., 2013a. Probing molecular associations of field-collected and laboratory-generated SOA with nano-DESI high-resolution mass spectrometry. J. Geophys. Res.: Atmos. 118 (2), 1042–1051.

O'Brien, R.E., Laskin, A., Laskin, J., Liu, S., Weber, R., Russell, L.M., Goldstein, A.H., 2013b. Molecular characterization of organic aerosol using nanospray desorption/electrospray ionization mass spectrometry: CalNex 2010 field study. Atmos. Environ. 68, 265–272.

Perraud, V., Horne, J.R., Martinez, A.S., Kalinowski, J., Meinardi, S., Dawson, M.L., Wingen, L.M., Dabdub, D., Blake, D.R., Gerber, R.B., Finlayson-Pitts, B.J., 2015. The future of airborne sulfur-containing particles in the absence of fossil fuel sulfur dioxide emissions. Proc. Natl. Acad. Sci. Unit. States Am. 112 (44), 13514–13519. http://dx.doi.org/10.1073/pnas.1510743112.

Pope III, C.A., Burnett, R.T., Thun, M.J., Calle, E.E., Krewski, D., Ito, K., Thurston, G.D., 2002. Lung cancer, cardiopulmonary mortality, and long-term exposure to fine particulate air pollution. Jama 287 (9), 1132–1141.

SCAQMD, 2013. Final 2012 air quality management plan. Tech. Rep. South Coast Air Quality Management District, Diamond bar, California Available at: http://www.aqmd.gov/home/library/clean-air-plans/air-quality-mgt-plan/final-2012-air-quality-management-plan.

Schiferl, L.D., Heald, C.L., Nowak, J.B., Holloway, J.S., Neuman, J.A., Bahreini, R., Pollack, I.B., Ryerson, T.B., Wiedinmyer, C., Murphy, J.G., 2014. An investigation of ammonia and inorganic particulate matter in California during the CalNex campaign. J. Geophys. Res.: Atmos.e 119 (4), 1883–1902. http://dx.doi.org/10.1002/2013JD020765.

Updyke, K.M., Nguyen, T.B., Nizkorodov, S.A., 2012. Formation of brown carbon via reactions of ammonia with secondary organic aerosols from biogenic and anthropogenic precursors. Atmos. Environ. 63, 22–31.

U.S. Environmental Protection Agency (EPA), 2009. Integrated Science Assessment for Particulate Matter (Final Report). Rep. EPA/600/R-08/139F. D. C, Washington.

Wang, X., Gao, S., Yang, X., Chen, H., Chen, J., Zhuang, G., Surratt, J.D., Chan, M.N., Seinfeld, J.H., 2010. Evidence for high molecular weight nitrogen-containing organic salts in urban aerosols. Environ. Sci. Technol. 44 (12), 4441–4446.

Wang, Y., Zhang, Q.Q., He, K., Zhang, Q., Chai, L., 2013. Sulfate-nitrate-ammonium aerosols over China: response to 2000–2015 emission changes of sulfur dioxide, nitrogen oxides, and ammonia. Atmos. Chem. Phys. 13 (5), 2635–2652. http://dx.doi.org/10.5194/acp-13. 2635–2013.

Warner, J.X., Dickerson, R.R., Wei, Z., Strow, L.L., Wang, Y., Liang, Q., 2017. Increased atmospheric ammonia over the world's major agricultural areas detected from space. Geophys. Res. Lett. 44 (6), 2875–2884. http://dx.doi.org/10.1002/2016GL072305.

Zhang, Y., Seigneur, C., Seinfeld, J.H., Jacobson, M., Clegg, S.L., Binkowski, F.S., 2000. A comparative review of inorganic aerosol thermodynamic equilibrium modules: similarities, differences, and their likely causes. Atmos. Environ. 34 (1), 117–137.